A Method for Flutter Detection by Infrared Imaging

Jorge Henrique Bidinotto[1,*], Eduardo Morgado Belo[1]

Bidinotto JH https://orcid.org/0000-0002-5352-2326

Belo EM https://orcid.org/ 0000-0002-1822-6337

ABSTRACT: The performance enhancement of aircraft coupled with the development of increasingly lightweight and flexible materials has led designers to use smaller structural safety factors along the time, which can make aerodynamic surfaces more susceptible to aeroelastic phenomena, including flutter. This kind of occurrence must be carefully investigated by ground and flight tests during aircraft development and certification, which requires suitable instrumentation in order to predict the occurrence of unwanted vibrations. The sensors in this kind of application must be less intrusive as possible, in order to not modify the dynamic or aerodynamic behavior of the system. This work proposes the use of infrared imaging as a tool for flutter detection, analyzing the suitability of the technique for this application. For this purpose, a literature review was performed by presenting infrared technology concepts; then, some preliminary tests were performed in a structure to predict flutter characteristics, and finally wind tunnel tests were executed in the same structure, validating this technique and highlighting its positive points and points that need improvement.

KEYWORDS: Flutter; Infrared imagery; Thermodynamics; Aeroelasticity.

INTRODUCTION

Some of the recent advances in aeronautical engineering are related to the use of lighter and more flexible materials in aircraft structures, which increases the performance of these vehicles and makes their manufacture easier. On the other hand, these advances can bring some disadvantages, such as increasing the susceptibility of structures to aeroelastic effects, such as flutter, besides the difficulty of carrying out tests to measure the flutter velocity of the structure.

To perform this kind of measure, it is necessary to use a set of accelerometers along its surface. According to McConnel and Varoto (2008), the weight of these sensors, however, may influence the result, becoming the test nonrepresentative, especially for light structures such as unmanned aerial vehicles or model airplanes for photographic applications. Additionally, the format can affect the aerodynamic flow through the surface.

Trying to minimize these problems, this paper proposes a flutter analysis that detects its occurrence based on temperature, which increases when the structure is in a condition close to flutter occurrence. This analysis is possible due to the fact that the structure deformation generates internal stresses, which results in a local temperature increase, detectable by infrared cameras (Bidinotto and Belo 2015). According to the same reference, the mechanical work executed in structure deformation can be converted in heat in a closed system. Nevertheless, the temperature variation is small, which requires an accurate experimental apparatus, as described along the text.

For theoretical background, Collar (1946) provided the first studies and the basic definition of aeroelasticity, with its very known diagram relating the interaction of aerodynamic, inertial and elastic forces, employed until today to explain this kind of phenomena.

Collar (1946), Bisplinghoff *et al.* (1995), Clark *et al.* (2004), and Hodges and Pierce (2002) provided the general basis of the aeroelasticity classical theory and the knowledge used in computer simulations aimed to provide speed and frequency of flutter occurrence, while Benini (2002), Marqui Junior and Belo (2004) and Costa (2007) described in details the aeroelastic models usage, while Nitzsche (2001) presented fundamental theories for designing new models for this application.

The National Test Pilots School (1995) and Gallagher *et al.* (1992) provided information about flight tests applied to aeroelastic phenomena, and Ward *et al.* (2006); van Nunen and Piazzoli (1979) and Olson (2000) showed the theoretical concepts applied in this kind of test. Flutter flight tests procedures were described by Brenner *et al.* (1997), Kehoe (1995), Lind (1997, 2003), Lind *et al.* (1998) and Wright *et al.* (2003), allowing knowledge of the state-of-the-art for these tests, as well as Marqui Junior *et al.* (2007), Sutherland (2008) and Suleman *et al.* (2002) provided practical studies and some laboratory wind tunnel for aeroelastic phenomena tests. The Federal Aviation Administration (FAA 2000) provides certification requirements for this type of testing and also the test guide (FAA 2018), demonstrating compliance with these requirements. The basic infrared radiation theory can be provided by Hudson Junior (1969), and its imaging use for temperature measurement can be seen in Holst (2003), while Wyatt (1987) explained design concepts for devices with this purpose.

Aeronautical applications for infrared imaging, including flight tests can be seen in McShea (2010), Clifton (1996) and Fisher *et al.* (2003), while applications on the aeronautical industry were described by Dehne *et al.* (2012), Fujino *et al.* (2003), FLIR Systems (2011, 2012a), aiming mainly thermal comfort and aerodynamic applications.

Malerba *et al.* (2008), Banks *et al.* (2000) and Zuccher *et al.* (2003) showed the same applications, in an academic way, while the best conditions for infrared imaging application are described by FLIR Systems (2012b) and Infrared Training Center (2008).

The present paper describes the theoretical fundamentals used on infrared imaging development. It also states the structure used and some preliminary tests performed to obtain its flutter characteristics, and shows the method for experimental validation, describing the procedures and its results.

INFRARED IMAGING

In electromagnetic spectrum (Fig. 1), the infrared radiation encompasses the part with a wavelength between 800 to 10^6 nm and is divided in short (wavelength of 800 to 1500 nm), medium (1500 to 5600 nm) and long radiation (5600 to 10^6 nm) (Holst 2003).
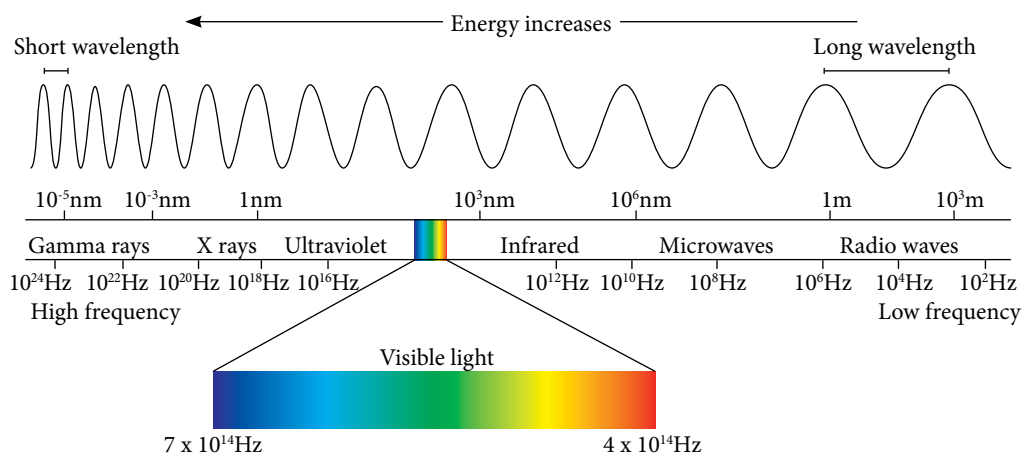
Figure 1. Electromagnetic spectrum. (Source: Bidinotto *et al.* 2013).

The images are possible by processing the infrared radiation emitted by an object using proper equipment (infrared cameras). The infrared radiation used for thermal analysis is generally of medium and long radiation. The bigger the temperature, the shorter the wavelength. These different wavelengths (and hence frequency) sensed by the camera are processed and generates images based on different radiation characteristics (Fig. 2).

Image   Infrared camera   Infrared image   Human eye
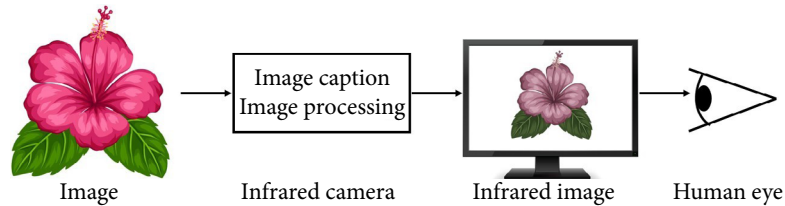
Figure 2. Image processing procedure.

This kind of analysis is possible due to some properties of thermal radiation:

- Any kind of body with a temperature above zero Kelvin emits thermal radiation;
- It can occur in any environment (even vacuum);
- It can cross gaseous environments;
- Normally cannot cross liquids or solids (with some few exceptions).

Another important issue is the fact that the radiation incident from the environment can be absorbed, reflected and a small part is able to cross (such as a lens) through the object. The law of total radiation (W) describes this principle and is represented by the Eq. (1) (Holst 2003):

$$W = \alpha W + \tau W + \rho W \tag{1}$$

$$\alpha + \tau + \rho = 1 \tag{2}$$

The coefficients represent the absorption of incident energy of the object (α), transmission (τ) and reflection (ρ), similarly to the radiation of visual light, with reflection, refraction, and transmission and have values between 0 and 1. For this reason, the operation principle of an infrared camera is similar to a visible light digital camera, with lenses to focus the radiation onto the detector and a set of electronic hardware and software to process the received signals, generating images (FLIR 2012b).

Therefore, the main advantage of thermography is to allow the analysis of the temperature of an entire object without physical contact. The analysis can be complete on a surface, as the detectors are composed of a focal plane array (FPA) of materials sensitive to a specific wavelength range. The number of sensors in the array can vary from about 160×120 to 1024×1024 pixels, allowing a resolution with more than 1 million individual detectors.

PRELIMINARY TESTS

For the experimental validation, a structure composed of a rigid wing fixed on the top of flexible support was used. The structure is shown in Fig. 3 and its details are described in Table 1.

The flexible support, consisted of a central beam and four axes, positioning an upper plate, designed to have a given flutter speed. The wind tunnel maximum speed is not enough to reach the wing flutter, considering the wing stricture rigidity; for this reason, the support was used to have the necessary flexibility to achieve the condition for this study.

Before the tests using infrared imaging to detect flutter, some preliminary tests were performed in order to measure the structure characteristics. Initially, an experimental modal analysis was performed to determine the frequency and vibration mode shapes using the traditional method to attest that the first and second modes natural frequency would be far from the third one. Then, a wind tunnel test was carried out for determining the speed and frequency of flutter in the structure. Both tests are described below.
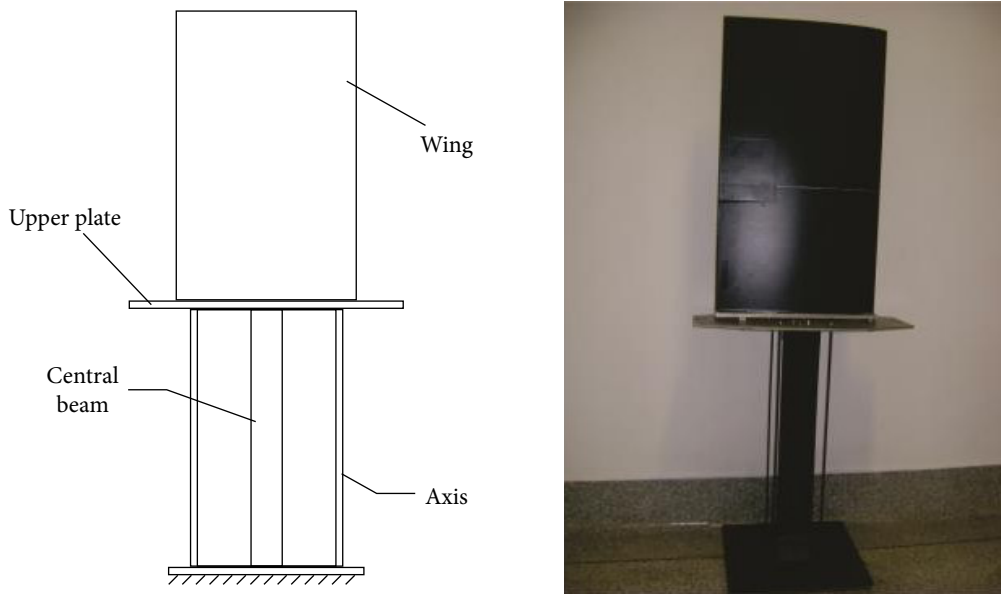
Figure 3. Images presenting the set used on this work.

Table 1. Structure properties.

Element	Material	Dimensions, mm	
Central beam	Steel alloy 1020	Length	700
		Width	100
		Thickness	2
Axis	Steel alloy 1020	Diameter	5.5
Upper plate	Aluminum alloy 2024T	Length	600
		Width	300
		Thickness	5.8
Wing NACA 0012	Aluminum alloy 2024T	Span	800
		Chord	450

EXPERIMENTAL MODAL ANALYSIS

Experimental modal analysis was performed in the central beam of the support, which is the part of the structure expected to give the set the rigidity characteristics. Due to structure limitations and the type of information to be measured, the excitation by impulse force hammer with discrete measurement points on the central beam was chosen, measuring one point at a time and changing the accelerometer position in order to add the least possible mass to the system, minimally affecting its inertial behavior.

According to McConnell and Varoto (2008) and Rao (1990), this kind of test is performed when the load applied to the structure must be low and has the advantage to having a small influence in the mass of the structure, becoming ideal for this case, despite the need of change the accelerometer position after each load application.

The experimental set scheme is shown in Fig. 4. The set support/wing (1) had its accelerations measured by an Accelerometer Kistler K-Beam, model 8303A10M4 (2), powered by a Kistler Sensor Power Supply, model 5210 (3). The structure was excited by an Impulse force hammer Kistler, model 9724A2000 (5), coupled by a Kistler Piezotron, model 5134 (6). All the data were sent to a Signal Calc card (4), connected to a laptop for data acquisition, with software SignalCalc 4.0 (7).
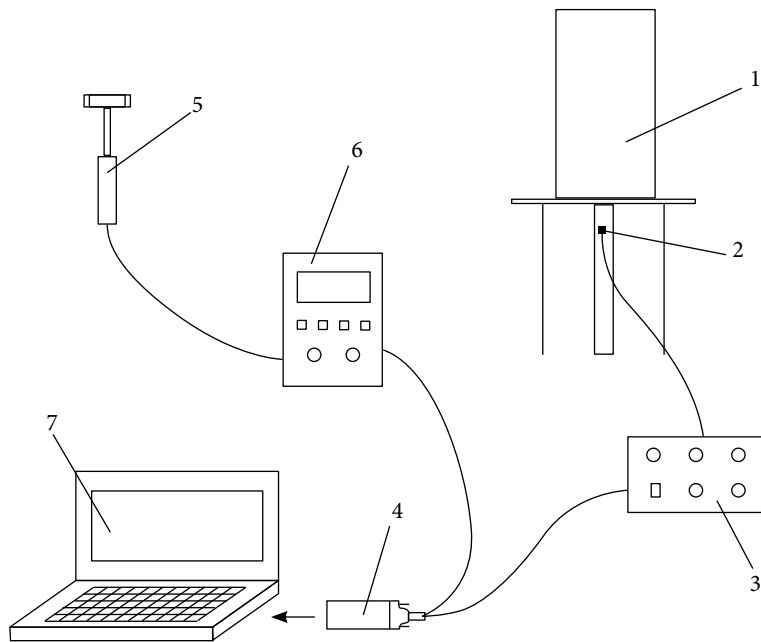
Figure 4. Experimental set for modal analysis.

The load application point is the wing aerodynamic center in the middle of the span as shown in Fig. 5 and the signal was measured at the points, which the support center beam was discretized, according to the scheme shown. For each measurement, the accelerometer had its position changed and a new excitation was performed.
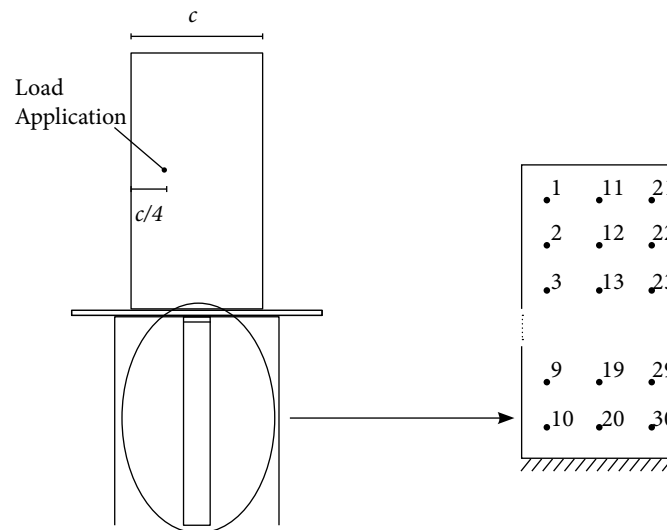
Figure 5. Central beam discretization.

Frequency response function (FRF) was extracted from the output, consisted by the accelerometer measurement (in grams), over the input, which was the impact force measured by the tip of the impulse force hammer (in Newtons). Figure 6 shows the plot of all 30 points on the same graph, where is possible to clearly observe three vibration modes, with the frequency values shown in Table 2.
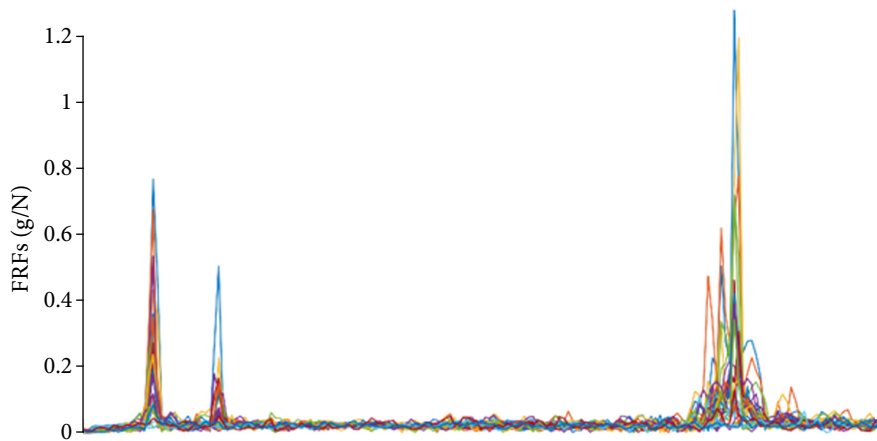
Figure 6. Frequency response functions measured.

Table 2. Vibration modes experimentally obtained.

Mode	Frequency (Hz)	Shape
1	1.5625	First flap bending
2	3.0273	First torsion
3	14.551	Second flap bending

The modal vector of each mode was plotted, which provides its shapes, using the FRF values from each point at the specified frequency. The results are shown in Figs. 7 to 9.
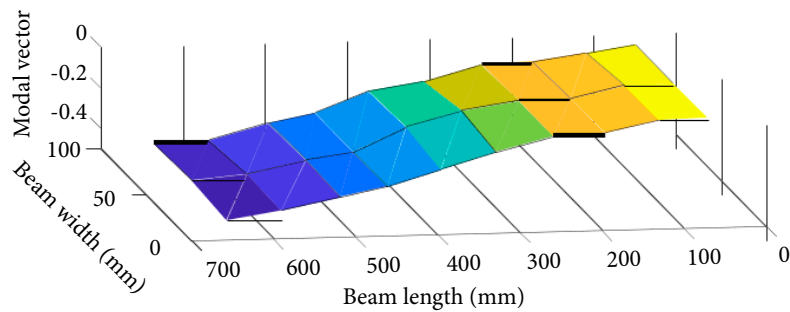
Figure 7. First mode shape experimentally measured.
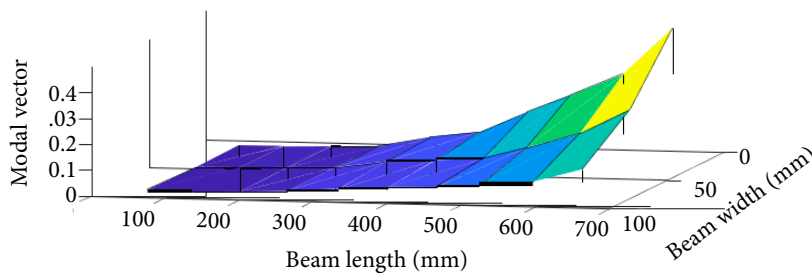
Figure 8. Second mode shape experimentally measured.
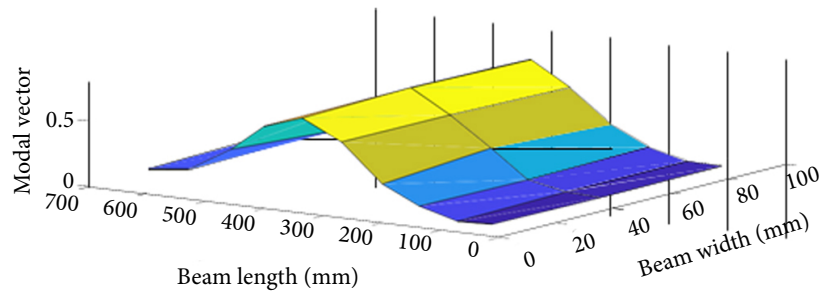
Figure 9. Third mode shape experimentally measured.

From the data experimentally obtained, it can be concluded that the analyzed structure is satisfactory for the experiment because it has two vibration modes with close frequencies and far from the third mode, characteristic observed in structures susceptible to flutter occurrence.

FLUTTER CHARACTERISTICS MEASUREMENT

In order to measure the structure flutter characteristics, such as frequency and speed, a study was performed where the set support/wing was tested in a wind tunnel, instrumented with an accelerometer (point 1, Fig. 5) detecting accelerations in flap bending and torsion. The experiment scheme is shown in Fig. 10a and an image of the mounted experimental apparatus in Fig. 10b.
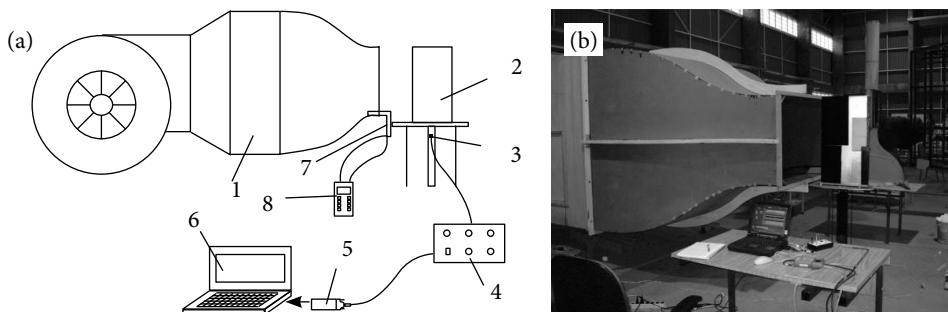
Figure 10. Experimental set for flutter characteristics determination scheme (a) and its picture (b).

In this set, an open circuit wind tunnel (1) provides airflow to the wing mounted on the set support/wing (2). Its accelerations were measured by an accelerometer Kistler K-Beam, model 8303A10M4 (3), powered by a Kistler sensor power supply, model 5210 (4) and the data was sent to a SignalCalc card (5), connected to a laptop for data acquisition, with software SignalCalc 4.0 (6). The flow characteristics were measured in real-time by a pitot tube (7) and a DPCalc Manometer, model 8705-M-GB (8).

Using this apparatus, the airspeed was changed and measured by pitot read in the manometer, and at each speed, a small displacement was caused on the wing, measuring its free response by the accelerometer output, plotted in Fig. 11 for various speeds.

From the measurements, it is possible to calculate the damping for each speed, based on the logarithmic decrement of the graph, as presented in Table 3.
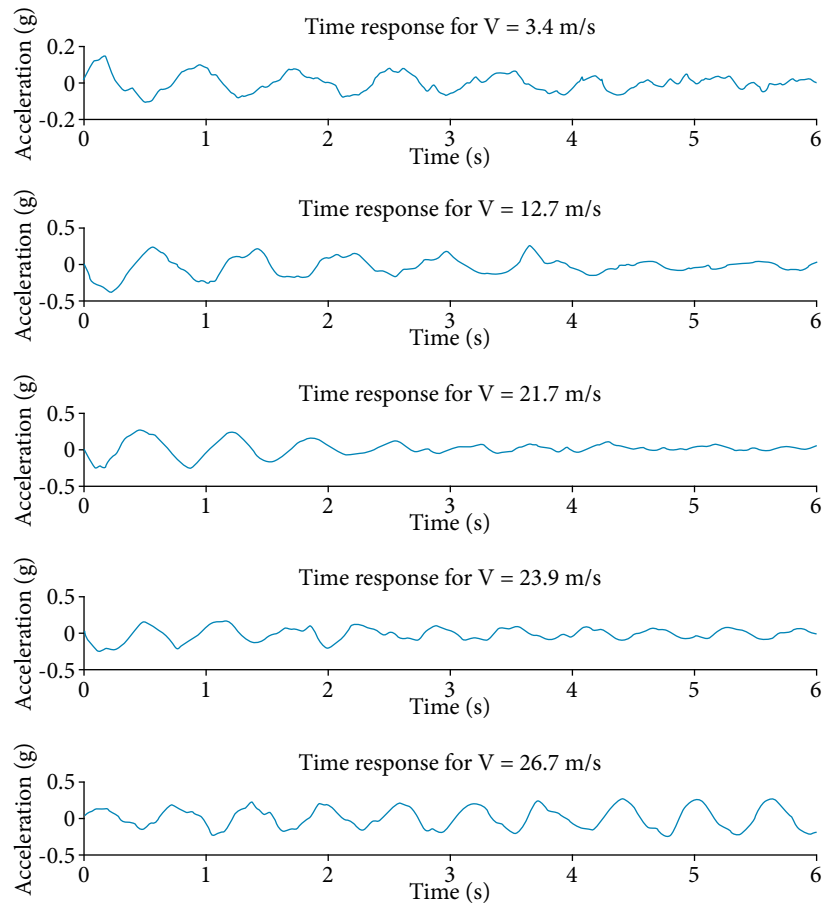
Figure 11. Time response for some of the tested speeds.

Table 3. Speeds tested and its damping calculated.

Airspeed (m/s)	Damping
3.8	0.057
8.3	0.052
12.7	0.050
17.3	0.046
19.5	0.040
21.7	0.033
23.9	0.015
26.7	-0.007

Then, it was possible to plot damping versus speed (Fig. 12). Adding a trendline obtained by interpolation to the plotted points. When the line is equal to zero (neutral damping), it is possible to calculate the system flutter speed, whose value is 25.6 m/s.

Figure 12. Damping versus airspeed collected data.

Damping versus airspeed
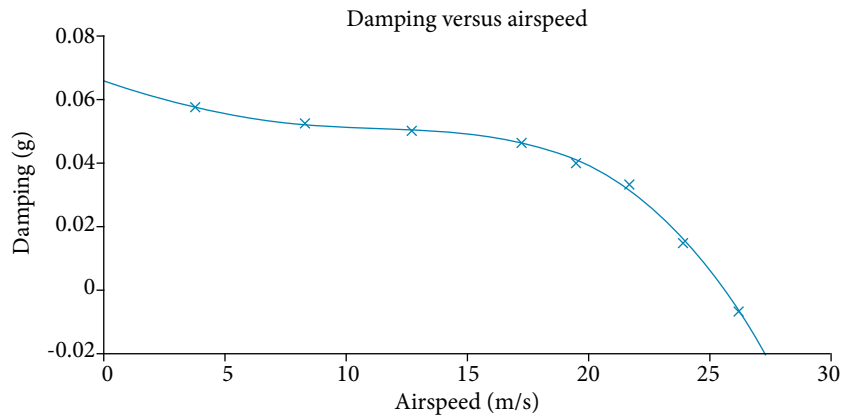
Figure 12. Damping versus airspeed collected data.

FLUTTER DETECTION USING INFRARED IMAGING

In order to validate the methodology of detecting flutter by infrared imaging, an experiment was performed using the same structure from the previous section. The wing was positioned in a wind tunnel and the central beam of the flexible support was recorded by an infrared camera. For some different airspeeds, images were recorded, as shown in the scheme in Fig. 13a and the picture in Fig. 13b.
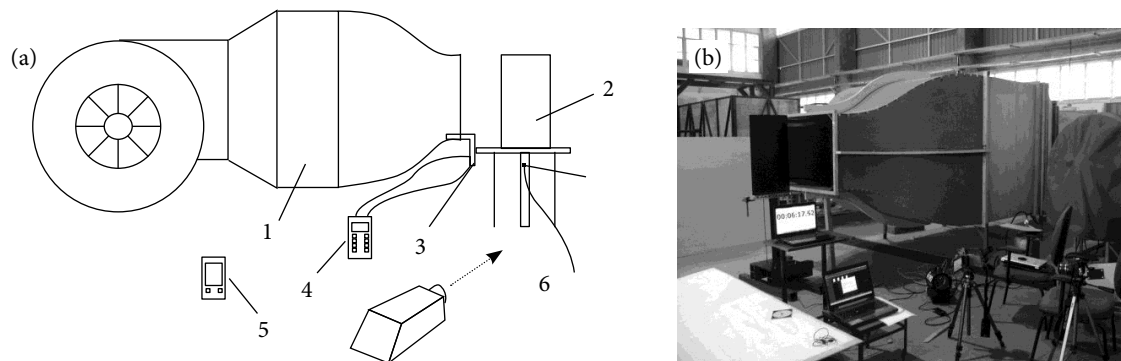
Figure 13. Scheme (a) and picture (b) from the experimental apparatus used for flutter detection with infrared imaging.

The open circuit wind tunnel (1) provides airflow to the wing mounted on the set support/wing (2). The airspeed was measured in real-time by a pitot tube (3) and a DPCalc Manometer, model 8705-M-GB (4), while the environmental conditions were controlled by a Portable weather station, model Instrutemp ITWH 1170 (5). For each airspeed, the support central beam was recorded by an Infrared Camera, model FLIR P620 (6).

According to Holst (2003), Malerba *et al.* (2008) and the Infrared Training Center (2008), temperature contrast is intensified if the structure is cooled. Hence, before each measurement, the central beam was cooled using a carbon dioxide fire extinguisher. Another relevant caution was to paint the central beam in mat black to minimize reflection effects.

Another positive factor, in this case, is that the recorded beam is not immersed in the aerodynamic flow which could difficult the visualization of contrast temperatures due to the thermal convection effect.

Figure 14 shows a series of infrared images from the structure in various airspeeds below the flutter condition: (a) 6.0 m/s; (b) 10.5 m/s; (c) 18.4 m/s, and (d) 20.6 m/s. It can be observed that the temperature distribution patterns and their values are very similar in all cases. All images shown in this figure are in the same range of colors and temperatures.
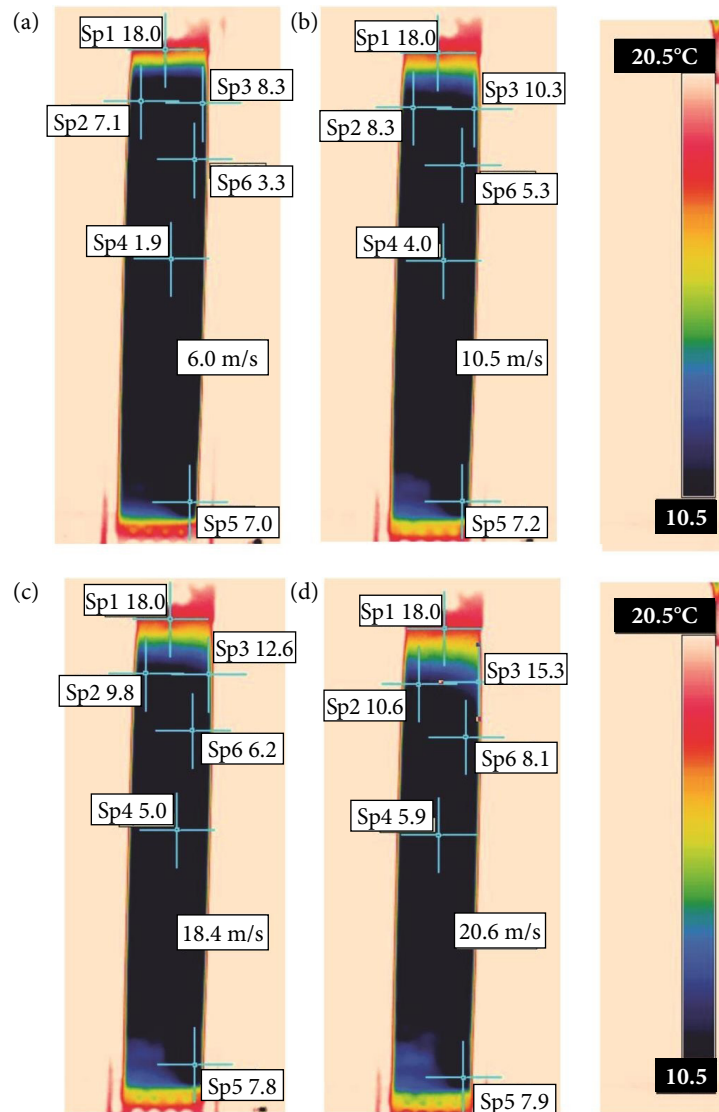
Figure 14. Infrared images in airspeeds below flutter speed.

It is noticeable through the analysis of the results that it is not possible to observe temperature change for different air speeds at the hottest points of the structure, because they are close to thermal equilibrium with the environment, as noted in sections marked as Sp1. By observing the Sp5 and Sp4 points, it is possible to conclude that there is a small temperature increase in cold points where a high-tension concentration is not expected, due to the heat exchange in function of time. At points where high stress is expected, the variation in temperature is more pronounced with increasing flow speed, as shown in points Sp2, Sp3, and Sp6. This temperature variation shows a pattern of bending, which can be observed by comparing the spots Sp3 and Sp6. A torsion pattern is also observed, if the Sp2 and Sp3 points are compared in addition to the color pattern on the upper end of the structure, as the speed increases.

Figure 15 shows images of the structure in flutter condition. In this case, the wing was exposed to an airspeed of 26.4 m/s. In this situation, several photos with infrared imaging were obtained, some of them are illustrated in this figure.
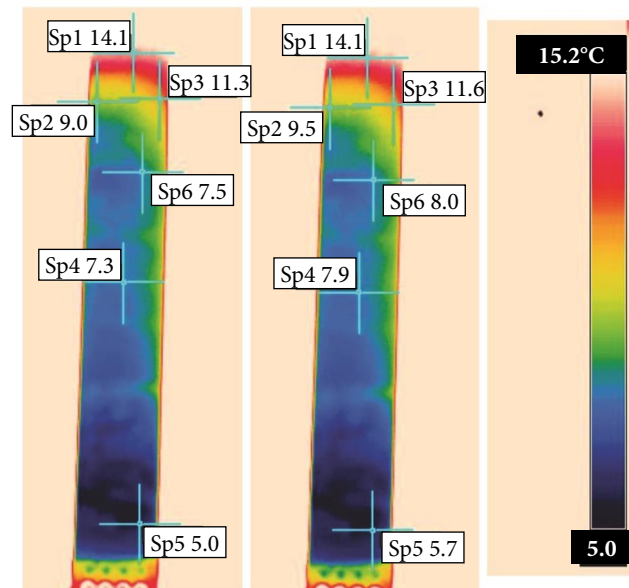
Figure 15. Infrared images in flutter speed.

It is important to note that the structure was cooled again before the test in flutter condition, allowing a homogeneous temperature throughout its surface. For this reason, Fig. 15 presents a new range of colors and the pattern of temperature distribution was again formed from a homogeneous condition.

It can be observed that the standard temperatures in flutter condition follow the same trend as the previous figures, but with more pronounced differences in temperature, making it easier to visualize. The same deformation patterns in bending and torsion can also be observed, by comparing the points in which temperature is measured numerically, similarly to the previous case.

One difference, however, may be observed in temperature patterns before and after reaching the flutter condition: the bottom of the beam (clamped side) is colder than the upper part, although a region where it is provided high-stress concentration.

This difference can be attributed to the fact that, due to flutter, the structure is in an oscillating movement, which leads to heat exchange by forced convection in its upper region, causing thermal equilibrium with environment quicker. The temperature difference along the surface of the structure allows identifying the stress concentration caused by the deformation and thus identifying the involved energy accumulation due to the occurrence of flutter. Therefore, it is considered that the method is suitable for identifying this phenomenon and some new developments must be performed before real applications in aircraft.

CONCLUSIONS

Analyzing this methodology, it can be preliminarily concluded that infrared imaging is a powerful tool for the detection of processes involving temperature variations and contrasts. These applications include flutter detection due to temperature increase in regions with tension increment, and the measurement of vibration mode shape in structures, with very consistent results.

The use of this technology for these purposes is important because it can eliminate the influence of the mass of the sensors in modal analysis and flutter tests, especially in lighter structures. Additionally, the time spent to this kind of tests can be greatly reduced using this methodology.

The method proved to be reliable and safe, and, with some improvements, it is possible to be used for flutter flight tests or other aeronautical applications, reducing time, cost and increasing safety.

Additionally, some challenges were faced during the execution and must be solved for future experiments, as the sample rate of the camera, that must be improved in order to obtain results from higher frequency vibration structures and the cooling process that must be changed to a more precise procedure, in order to obtain the temperature homogeneity before the test.

For future work, a subroutine can be developed to provide the temperature numerical values in some points of the structure in real-time during the test.

ACKNOWLEDGMENTS

FUNDING

AUTHOR'S CONTRIBUTION

Conceptualization, Bidinotto, J. H.; Methodology, Bidinotto, J. H.; Investigation, Bidinotto, J. H. and Belo, E. M.; Writing – Original Draft, Bidinotto, J. H.; Writing – Review and Editing, Bidinotto, J. H. and Belo, E. M.; Resources, Bidinotto, J. H. and Belo, E. M.; Supervision, Belo, E. M.

REFERENCES

[FAA] Federal Aviation Administration (2000) Code of Federal Regulations. Washington: U.S. Government Printing Office. [accessed Jan 22 2013]. https://www.ecfr.gov/cgi-bin/text-idx?SID=fac5240ded548b3506e2fe02f6f5ab84&mc=true&tpl=/ecfrbrowse/Title14/14cfr25_main_02.tpl

[FAA] Federal Aviation Administration (2018) AC 25-7D (Cancelled) - Flight test guide for certification of transport category airplanes. Washington: U.S. Government Printing Office. [accessed Oct 28 2018]. https://www.faa.gov/regulations_policies/advisory_circulars/index.cfm/go/document.information/documentID/1033309

Banks DW, van Dam CP, Shiu HJ, Miller GM (2000) Visualization of In-flight flow phenomena using infrared thermography. NASA TM-2000-209027. Dryden: NASA. [accessed Apr 17 2013]. https://ntrs.nasa.gov/archive/nasa/casi.ntrs.nasa.gov/20000079999.pdf

Benini GR (2002) Modelo numérico para simulação da resposta aeroelástica de asas fixas. (Dissertation). São Carlos: Universidade de São Paulo.

Bidinotto JH, Belo EM (2015) Modal shape analysis using thermal imaging. J Aerosp Technol Manag 7(2):185-192. https://doi.org/10.5028/jatm.v7i2.450

Bidinotto JH, Kleinubing M, Catalano FM, Belo EM (2013) Thermography applied on boundary layer transition visualization. Paper presented 22nd International Congress of Mechanical Engineering (COBEM 2013). COBEM; Ribeirão Preto, Brazil.

Bisplinghoff RL, Ashley H, Halfman RL (1955) Aeroelasticity. Cambridge: Addison-Wesley Publishing.

Brenner MJ, Lind RC, Voracek DF (1997) Overview of recent flight flutter testing research at NASA Dryden. NASA TM-4792. Dryden: NASA. [accessed Apr 25 2013]. https://ntrs.nasa.gov/archive/nasa/casi.ntrs.nasa.gov/19970015518.pdf

Clark R, Cox D, Curtiss Junior HC, Edwards JW, Hall KC, Peters DA, Scanlan R, Simiu E, Sisto F, Strganac TW (2004) A modern course in aeroelasticity. 4th ed. Dordrecht: Springer. https://doi.org/10.1007/1-4020-2106-2

Clifton JM (1996) Introduction to avionics flight test. AGARD 15. [accessed Sep 15 2014]. https://apps.dtic.mil/dtic/tr/fulltext/u2/a322378.pdf

Collar AR (1946) The Expanding Domain of Aeroelasticity. Aeronaut J 50(428):613-636. https://doi.org/10.1017/S0368393100120358

Costa TFG (2007) Estudo numérico de uma asa com controle ativo de 'flutter' por realimentação da pressão medida num ponto (Dissertation). São Carlos: Universidade de São Paulo.

Dehne T, Bosbach J, Heider A (2012) Dynamics of aircraft cabin ventilation studied by in-flight infrared thermography. Paper presented 11th International Conference on Quantitative InfraRed Thermography. QIRT; Naples, Italy. https://doi.org/10.21611/qirt.2012.209

Fisher D, Horstmann KH, Riedel H (2003) Flight test measurement techniques for laminar flow. AGARDograph 300. Flight Test Techniques Series – Volume 23. Washington: RTO/NATO. [accessed Sep 15 2014]. https://apps.dtic.mil/sti/pdfs/ADA419418.pdf

FLIR Systems (2011) Application Story – DLR Dornier 228. Hong Kong: FLIR.

FLIR Systems (2012a) Application Story – Dassault Falcon 7X. FLIR Advanced Thermal Solutions. France: FLIR.

FLIR Systems (2012b) The ultimate infrared handbook for R&D professionals: A resource guide for using infrared in the research and development industry. Wilsonville: FLIR.

Fujino M, Yoshizaki Y, Kawamura Y (2003) Natural-laminar-flow airfoil development for a lightweight business jet. J Aircraft 40(4):609-615. https://doi.org/10.2514/2.3145

Gallagher GL, Higgins LB, Khinoo LA, Pierce PW (1992) U.S. Naval Test Pilot School Flight Test Manual: Fixed wing performance. Contract N00421-90-C-0022.

Hodges DH, Pierce GA (2002) Introduction to structural dynamics and aeroelasticity. Cambridge: Cambridge University Press. https://doi.org/10.1017/CB09780511809170

Holst GC (2003) Electro-optical imaging system performance. 3rd ed. Oviedo: JCD Publishing.

Hudson Junior RD (1969) Infrared system engineering. New York: Wiley-Interscience.

Infrared Training Center (2008) Curso de termografia Nível I. Infrared Training Center; São Paulo, Brazil.

Kehoe MW (1995) A historical overview of flight flutter testing. NASA TM-4720. Dryden: NASA. [accessed Aug 27 2014]. https://ntrs.nasa.gov/archive/nasa/casi.ntrs.nasa.gov/19960004074.pdf

Lind RC (1997) A presentation on robust flutter margin analysis and a flutterometer. NASA TM-97-206220. Dryden: NASA. [accessed Aug 12 2014]. https://ntrs.nasa.gov/archive/nasa/casi.ntrs.nasa.gov/19970037547.pdf

Lind RC (2003) Flight-test evaluation of flutter prediction methods. J Aircraft 40(5):964-970. https://doi.org/10.2514/2.6881

Lind RC, Freudinger LC, Voracek DF (1998) Comparison of aeroelastic excitation mechanisms. J Aircraft 35(5):830-832. https://doi.org/10.2514/2.7585

Malerba M, Argento M, Salviuolo A, Rossi GL (2008) A boundary layer inspection on a wing profile through high resolution thermography and numerical methods. WSEAS Trans Fluid Mech 3(1):18-28.

Marqui Junior C, Belo EM (2004) Estudo teórico e experimental de um controlador para supressão de flutter (Dissertation). São Carlos: Universidade de São Paulo.

Marqui Junior C, Rebolho DC, Belo EM, Marques FD, Tsunaki RH (2007) Design of an experimental flutter mount system. J Braz Soc Mech Sci & Eng 29(3):246-252. https://doi.org/10.1590/S1678-58782007000300003

McConnell KG, Varoto PS (2008) Vibration testing: theory and practice. 2nd ed. Hoboken: John Wiley & Sons.

McShea RE (2010) Test and evaluation of aircraft avionics and weapon systems. Raleigh: SciTech Publishing. https://doi.org/10.2514/4.867606

National Test Pilots School (1995) Introduction to FW performance & flying qualities flight testing. 2nd ed. Mojave.

Nitzsche F (2001) Introductory aeroelasticity. Material de curso ministrado no LAE. São Paulo: USP.

Olson WM (2000) Aircraft performance flight testing. California: Air Force Flight Test Center.

Rao SS (1990) Mechanical vibrations. 2nd ed. Boston: Addison-Wesley.

Suleman A, Crawford C, Costa AP (2002) Experimental aeroelastic response of piezoelectric and aileron controlled 3D wing. J Intell Mater Syst Struct 13(2-3):75-83. https://doi.org/10.1177/104538902761402477

Sutherland AN (2008) A small scale pitch-plunge flutter model for active flutter control research. Paper presented 26th International Congress of the Aeronautical Sciences. ICAS; Anchorage, United States. [accessed Oct 02 2014]. http://www.icas.org/ICAS_ARCHIVE/ICAS2008/PAPERS/385.PDF

van Nunen JWG, Piazzoli G (1979) Aeroelastic flight test techniques and instrumentation. AGARD 9. [accessed Oct 10 2014]. https://apps.dtic.mil/sti/citations/ADA065938

Ward DT, Strganac TW, Niewoehner R (2006) Introduction to flight test engineering. 3rd ed. Dubuque: Kendall Hunt Publishing.

Wright JR, Wong J, Cooper JE, Dimitriadis G (2003) On the use of control surface excitation in flutter testing. Proc Inst Mech Eng G J Aerosp Eng 217(6):317-332. https://doi.org/10.1243/095441003772538589

Wyatt CL (1987) Radiometric system design. New York: The Free Press.

Zuccher S, Saric WS, Reed HL, McNeil LR (2003) The Role of Infrared Thermography in the Study of Crossflow Instability at M=2.4. Paper presented 7th Int Symp on Fluid Control, Measurement and Visualization. FLUCOME; Sorrento, Italy. [accessed Oct 05 2014]. http://profs.sci.univr.it/zuccher/downloads/ZSSWREML_FLUCOME2003.pdf